Original Article
Cite This: Colloid & Nanoscience Journal 1 (2023) 26-38.
CNJ.araku.ac.ir

# A periodic DFT study on superior adsorption of an azo dye over $B_3O_3$ monolayer

**Rezvan Rahimi [1, 2]*, Mohammad Solimannejad[1, 2]***

**Received:**2022-12-14
**Revised:** 2023-02-28
**Accepted:** 2023-02-28
DOI: **10.52547/CNJ.1.1.26**

[1] Department of Chemistry, Faculty of Science, Arak University, Arak 38156-8-8349, Iran
[2] Institute of Nanosciences and Nanotechnology, Arak University, Arak 38156-8-8349, Iran

**Abstract**

The objectives of this DFT study are to consider the adsorption properties of the 4-[2-[4-(dimethylamino) phenyl] diazenyl]-benzoic acid (p-methyl red) dye molecule on the pristine $B_3O_3$ semiconducting layer for potential application in dye-sensitized solar cells. Adsorption of dye molecules on different positions of the $B_3O_3$ nanosheet leads to the formation of the complexes with favorable adsorption energy in the range of -0.25 to -1.48 eV and the 50 to 57% percentage of change in band gap energy of the monolayer. The dye molecule is adsorbed in two forms on the $B_3O_3$ surface, the complexes of the trans-isomer with a more negative adsorption energy of -1.48 eV being more stable than -1.41 eV of the cis-isomer complexes. By the adsorption of dye molecules on the pristine $B_3O_3$ surface, the electronic properties of the surface change a lot, which in this work can be proved with the percentage of the changes in the gap energy of more than 50%. The present study results show that the studied substrate may be suitable for application in dye-sensitized solar cells via pairing with a desired dye molecule.

**Keywords:** $B_3O_3$ monolayer; Solar cell; DSSC; DFT study

## 1. Introduction

Photovoltaics (PV) is a technology for generating electrical power by converting solar radiation into direct current electricity using semiconductors. Photovoltaic power generation employs solar panels composed of solar cells containing a photovoltaic material. Solar photovoltaic power generation has long been a clean, sustainable energy technology [1]. The direct conversion of sunlight to electricity occurs without any environmental emissions during operation; thus it is eco-friendly. Depending upon the absorbing material used, manufacturing technique/process adopted, type of junction formed, etc., the solar cell technologies can be broadly classified as follows: (1) Wafer based crystalline silicon solar cells, (2) Thin-film solar cells, and (3) dye-sensitized solar cells (DSSCs). DSSCs are solar cells with low-cost materials and easy fabrication, belonging to the third generation of solar cells, and are designed to combine the advantages of both the first and second types. Grätzel and O'Regan discovered DSSCs in 1991 [2-5]. They are based on nature's principles of photosynthesis. The spectral response of stable wide band gap semiconductors like $TiO_2$ can be extended to visible light by sensitization with a dye molecule. In dye-sensitized solar cells (DSSCs), dye molecules adsorbed on the surface of the semiconductor are applied to transform light energy into electrical energy [2, 5-7]. The great advantage of this new type of solar cell is its ease of fabrication from cheap materials and the consequently low price. So far, research has been done on the advancement of DSSC technology, both experimentally and theoretically [8-16]. In most theoretical studies, the dye/$TiO_2$ interface has been used in the anode of DSSC [17-21].

So far, no studies concerning solar cells have been performed on $B_3O_3$ nanosheets. For this desired synthesized nanosheet, CO2 capture capacity [22], TEPA anti-cancer drug carrier properties [23], and dual application of the B3O3 nanosheets in sensing of COVID-19 biomarkers and drug delivery for treatment purposes [24] have been studied previously by the present authors. So, this sheet has been selected as a semiconductor in photo anode for DSSCs with no structural manipulations. The optimized structural properties of this synthesized nanosheet resulting from experimental [25] and theoretical [26] research in the past include powerful covalent B–B bonds of planar hexagons, six-fold symmetry due to the condensation of three tetrahydroxydiboron molecules and B=$O_3$ hexagons joining, hole with a surface area of 23 $Å^2$ and 6.27 Å diameter due to the correlation of six $B_3O_3$ units, and wide indirect band gap. The adsorption of various alkalis on considered nanosheets has been studied previously [27]. Hence, we plan to survey the dye/$B_3O_3$ interface's potential performance as an alternative to the dye/$TiO_2$ and other substrates.



Corresponding Authors: Rezvan Rahimi, Mohammad Solimannejad
r.rahimi1989@gmail.com
m-solimannejad@araku.ac.ir

Azo dye molecules have applications in textile and coating industries thanks to consistency, vivid color, high molar extinction, and economics [28-30]. Recently, they have been used to convert energy from light to electricity in dye-sensitized solar cells [31, 32]. Hitherto, the performance of p-methyl red azo dyes as a coating on $TiO_2$ anode in DSSCs has been evaluated [20, 21]. In the present manuscript, p-methyl red [4-[2-[4-(dimethylamino) phenyl] diazenyl]-benzoic acid] dye is used to probe its adsorption on $B_3O_3$ surfaces as an anode in DSSCs and subsequently impact of resulting electronic properties changes on the performance of dye-sensitized solar cells (DSSCs).

## 2. Computational details

All the calculations in this work have been performed using the DFT code DMol$^3$ in the Materials Studio package [33-35]. Electron exchange and correlation were treated within the generalized gradient approximation in PBE functional by Grimme's van der Waals (vdW) (DFT-D) correction [36-38] with the localized double-numerical basis with polarization functions (DNP) [39]. For our calculations, we have employed a k-point mesh of 9 × 9 × 1, a cut-off of 5.1 Å, a Fermi smearing of 0.005 Eh (1 Eh = 27.2114 eV), and a vacuum space of 20 Å. The appropriateness of our computational method has been confirmed in previous studies [22-24, 40-55]. The adsorption energy ($E_{ads}$) of dye molecule on pristine $B_3O_3$ surface is formally defined as:

$$E_{ads} = E_{dye/surf} - E_{surface} - E_{dye} \quad (1)$$

$E_{dye/surf}$, $E_{surface}$, and $E_{dye}$ indicate the electronic energies of dye/$B_3O_3$ complexes, pristine $B_3O_3$ surface, and isolated dye molecule, respectively.

Interaction energy which is the difference between the total electronic energy of the complex and the electronic energy of the deformed reacting species is calculated from the following equation;

$$E_{int} = E_{dye/surf} - E_{surface\text{-}D} - E_{dye\text{-}D} \quad (2)$$

$E_{surface\text{-}D}$ and $E_{dye\text{-}D}$ denote energies of deformed structures of the surface and dye, respectively. The deformation energy ($E_{def}$) is a discrepancy between the $E_{ads}$ and $E_{int}$ in the system. The percentage changes ($\%\Delta E_g$) in the $E_g$ is given by equation 3:

$$\%\Delta E_g = \left[\frac{(Eg_2 - Eg_1)}{Eg_1}\right] \times 100 \quad (3)$$

The $E_{g1}$ and $E_{g2}$ signify the initial and subsequent values of the band gap ($E_g$) of the $B_3O_3$ surface, respectively. We analyzed the effect of solvation on the interactions of the dye molecule with semiconductors by the conductor-like screening model (COSMO) of solvation [56, 57] implemented in DMol$^3$. The dielectric COSMO model is embedded in a molecule-shaped cavity surrounded by a dielectric ambiance with a given dielectric constant $\epsilon$.

## 3. Results and discussion

### 3.1. Geometry optimization of the pristine $B_3O_3$ nanosheet and the dye molecules

The unifying theme of this research is to exploit computational methods to illuminate the processes at work in DSSCs, to provide valuable insights towards improving device efficiency. Fig. 1 exhibits the optimized lattice parameters and bond lengths for the pristine $B_3O_3$ surface. Good agreement can be seen between the present calculated data and previous studies [27]. After complete optimization, the p-methyl red dye molecule is stabilized in two isomers, trans and cis, which according to the total energy -894.62 and -894.59 Ha, the trans-isomer is more stable than the cis-isomer. The optimal structure and molecular electrostatic potential (MEP) plots of the dye molecule in these two forms are shown in Figure 2. The optimized bond length of the dye molecule is N2–N3 (azo molecule) (1.279/1.263 Å for trans/cis isomers), C-C (Aromatic ring) (1.4 Å), C–N1 (1.45 Å), C-O1 (carbonyl group) (1.223 Å), C-O2, and O2-H (carboxylic acid group) (1.372 Å) and (0.977 Å), respectively. The reactivity of the considered dye molecule can be studied more by MEP plots, as shown in Figure 2 (c and d) for two forms, trans and cis. The negative domains of electrostatic potential (red color) are localized on the N and O atoms in both configurations. In contrast, H and C atoms of dye molecules have the most positive electrostatic potential (blue color).

Moreover, the MEP plot of the p-methyl red dye molecule in both forms shows that the carboxylic acid group's oxygen atoms and the azo molecule's nitrogen atoms are the potential sites to participate in nucleophilic attack to the pristine $B_3O_3$ surface. All calculated properties for the studied dye molecule are wholly consistent with the previous research on this dye molecule [20, 21]. First, we look at the adsorption properties of this nanosheet toward the p-methyl red dye molecule in both forms.

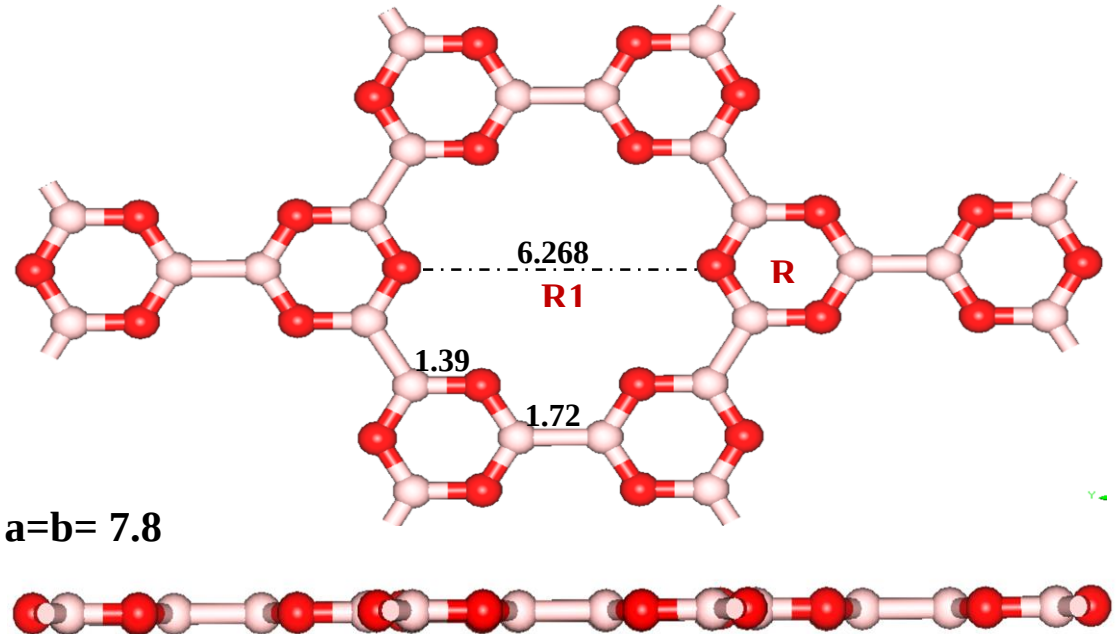


**Fig. 1.** Top and side views of the optimized structure of $B_3O_3$ nanosheet in Å. The B and O atoms are colored in pink and red balls, respectively.

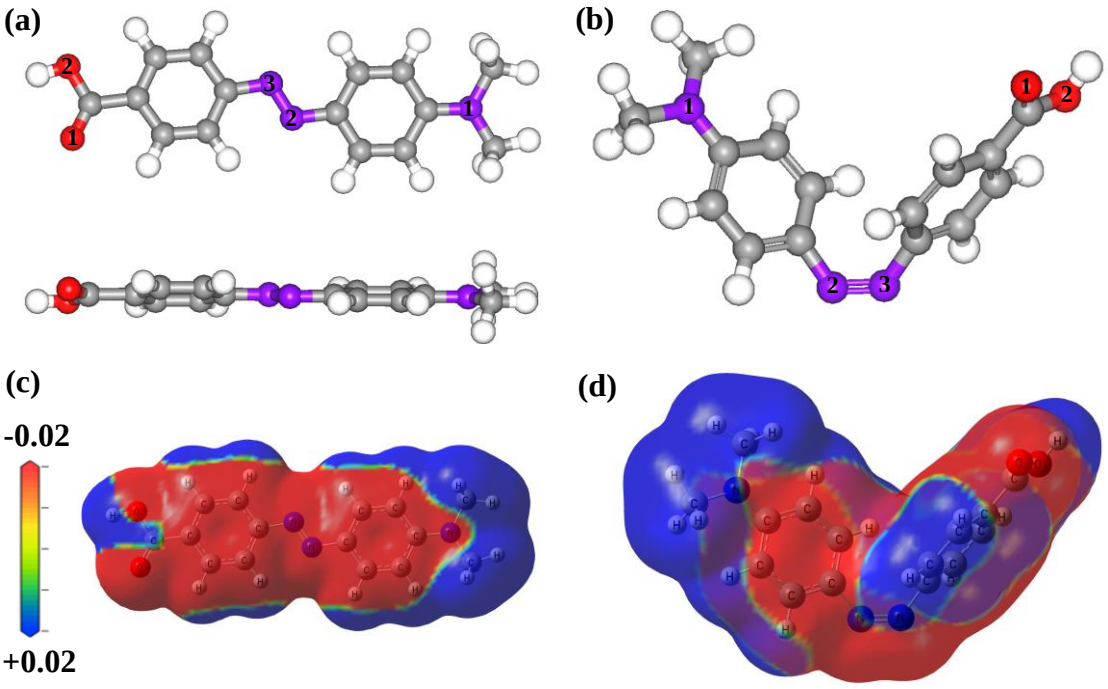


**Fig. 2.** Top and flank vision of optimized P-methyl red dye molecules in (a) trans and (b) cis forms and MEP surface of the (c) trans and (d) cis forms of the optimized dye molecules at ± 0.02 a.u. isosurface. The N, C, H, and O atoms are painted in purple, gray, white, and red balls.

## 3. 2. P-methyl red molecule adsorption on the pristine $B_3O_3$ nanosheet

Numerous binding modes exist between the dye molecule and the $B_3O_3$ surface. Various adsorption sites over the $B_3O_3$ surface are B and O atoms, B-O and B-B bonds, and R1 and R2 rings, as shown in Figure 1. Because of the carboxyl group and nitrogen atoms of the azo molecule in the structure of the dye molecule, the dye adsorption on the $B_3O_3$ nanosheet can occur through solid bonding between the O and N atoms of the dye with B and O atoms of the surface. According to this, primitive adsorption configurations were created by putting the O and N atoms of the dye on top or parallel to disparate adsorption sites of the $B_3O_3$. Then, for each primitive configuration, full geometrical optimizations without any symmetry constraint were performed, and after relaxation, the most stable structures were identified by comparing the obtained adsorption energy ($E_{ads}$). The dye molecule is adsorbed in two forms, trans and cis, on the $B_3O_3$ surface, the trans form with more negative adsorption energy being more stable than the cis form. However, we thoroughly evaluate the adsorption of both configurations on the surface (Fig. 3).

Initially, we placed the dye molecule in a trans form on all surface positions with all possible scenarios. Finally, only four stable complexes were obtained with absorption energies of -1.48, -0.62, -0.53, and -0.25 eV for the S1, S2, S3, and S4 complex, respectively. Two different forms of adsorption configurations were distinctive for the trans-dye/$B_3O_3$ complexes: interaction of the trans-dye molecule on $B_3O_3$ nanosheet in the (**I**) horizontal (S1 complex) and (**II**) vertical (S2-S4 complexes) positions with the surface. In the S1 complex, the trans-dye molecule is horizontal to the surface. The N1 atom and the azo molecule are located above the B atom and the R1 ring of the surface, respectively. The hydrogen atom of the carboxyl group is inclined towards the center of the R1 ring on the $B_3O_3$ surface. The vertical interval of the N1 atom in the dye with the B atom on the surface is 2.744 Å. In the S2 complex, the carboxyl group in the dye molecule with the B-O bond directly interacts at the surface. The oxygen atom in the carbonyl group interacts with the boron atom, and the hydrogen atom interacts with the oxygen atom of the $B_3O_3$ surface. The calculated bond length of $O1_{dye}$-$B_{surf}$ and $O\cdots H_{dye}$-$O_{surf}$ in the S2 complex is 1.669 Å and 1.605 Å, respectively. The O atom of the carbonyl group in the dye molecule interacts with the B atom on the surface in the S3 complex ($O1_{dye}$-$B_{surf}$ = 2.319 Å). In the S4 complex, the carboxyl group in the center of the R1 ring is stabilized above the surface. In this complex, the distance between the oxygen atom of the carbonyl group in the dye and the O atom of the R1 cavity on the surface is 3.029 Å.

When we optimize the cis-dye molecule overall positions of the surface, only three stable structures (S´1, S´2, S´3 complexes) with adsorption energies of -1.41, -0.98, and -0.62 were obtained, respectively. In the S´1 complex, N atoms of the cis-dye molecule are parallel, while the carboxyl group is vertical to the surface ($N2_{dye}$-$B_{surf}$ =3.086 Å). In contrast to the S´1 structure, in the S´2 complex, the carboxyl group is stabilized parallel to the surface with an interaction distance of 1.715 Å between the N3 atom of the dye and the B atom of the surface. In the cis-dye molecule, the N1 atom and COOH group of dye is located upwards, but the azo molecule of the cis-dye is inclined downwards in the S´3 complex ($N2_{dye}$-$B_{surf}$ =2.575 Å). Because of this, the S1 and S´1 complexes have the most negative adsorption energy. The most stable dye/$B_3O_3$ complexes are S1 (trans) and S´1 (cis), with $E_{Ads}^{Gas}$ -1.48 and -1.41 eV, respectively. These features are utterly consistent with the results of the MEP analysis in Fig. 2.

It is interesting to notice that the Eads of dye/$B_3O_3$ complexes are considerably smaller than their Eint due to the dye molecule's and surface's considerable deformation. The S2 (trans) and S´2 (cis) complexes have the highest value of $E_{int}$ (−1.69 eV and -1.86 eV) among the other configuration (see Table 1), which shows that the deformations of the dye molecule and the surface are substantial. In the S2 complex, the strong hydrogen bond is formed between the trans-dye and surface ($H_{dye}$-$O_{surf}$), and the COOH group of trans-dye is more active than the other atoms in the reaction with the surface. While the strong bond is formed between the azo molecule of cis-dye and the surface ($N3_{dye}$-$B_{surf}$), and the azo group of cis-dye is the most active site in the reaction with the surface. The calculated values of $E_{int}$ for dye/$B_3O_3$ complexes are -1.65, -1.69, -0.7, and -0.38 eV for S1, S2, S3, and S4 complexes, while for S´1, S´2, S´3 complexes are -1.55, -1.86, and -0.79 eV, respectively (see Table 1). The maximum values of $E_{def/surf}$ (0.83 eV/0.79 eV) and $E_{def/dye}$ (0.24 eV/0.08 eV) in trans/cis forms of the dye molecule are related to S2 (trans) and S´2 (cis) complexes. Complex S´2 (cis) is more stable than S2 (trans), and at the same time, the deformations of the surface and dye of the S2 are much more than the S´2 complex.

**S1**

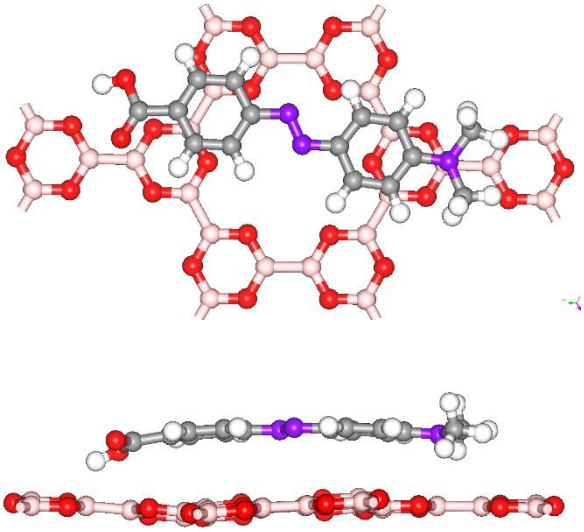

**S2**

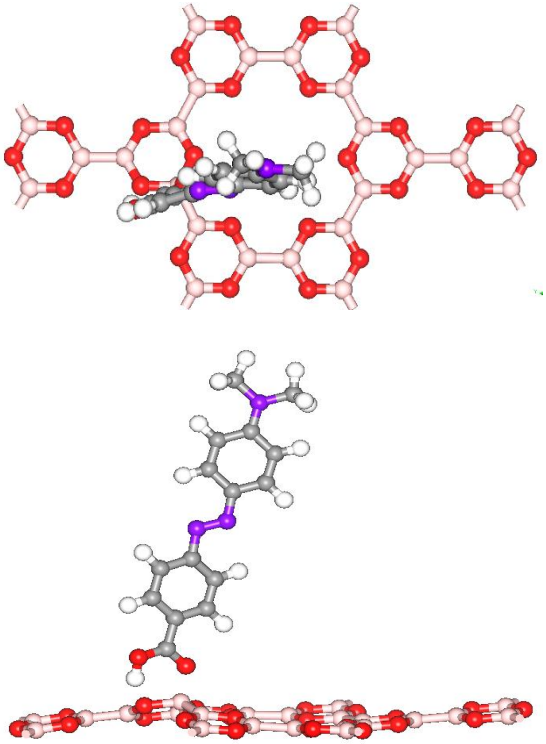

**S3**

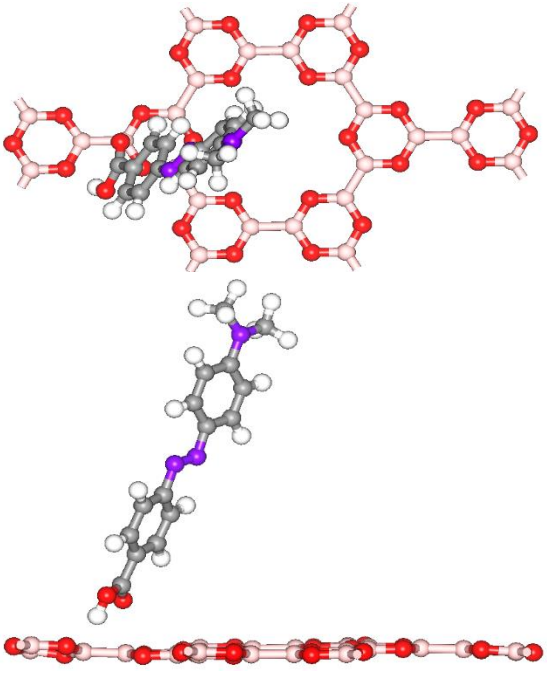

**S4**

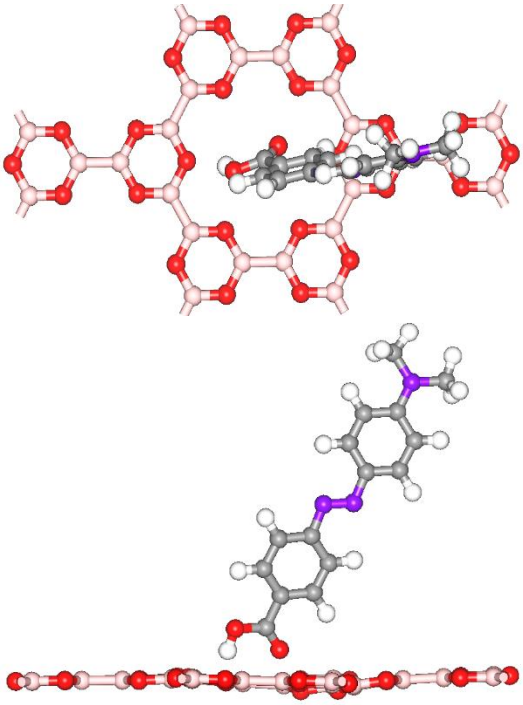

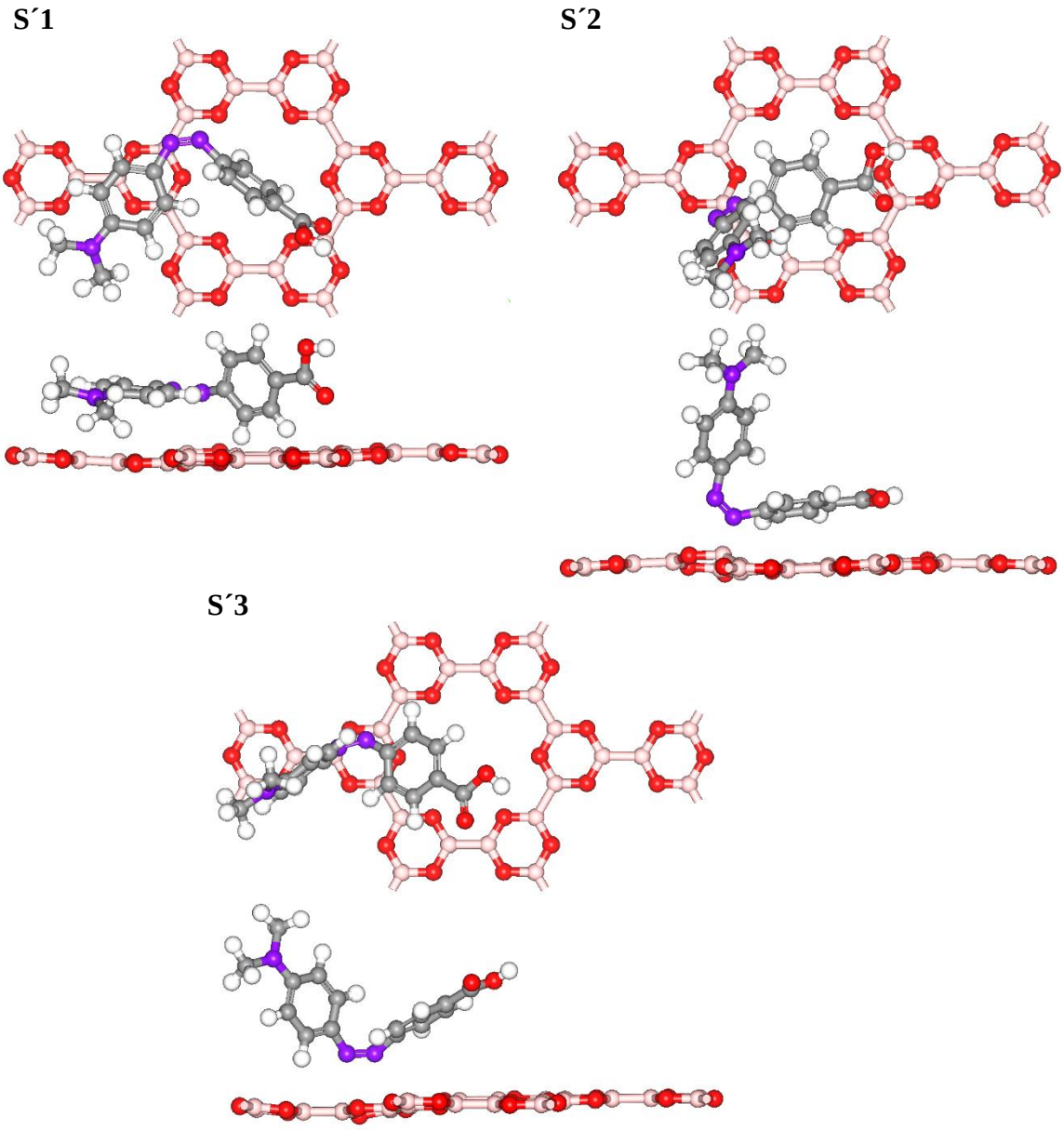


**Fig. 3.** Top and side views of the four and three stable configurations of dye molecule of (S1-S4) trans-P-methyl red and (S´1- S´3) cis-P-methyl red adsorbed on the $B_3O_3$ nanosheet. The B, N, C, H, and O atoms are painted in pink, purple, gray, white, and red balls.

The electronic properties of the surface before and after the adsorption of the dye molecule in two trans, and cis isomers, have been investigated through band-structure (BS) analysis. The Fermi level was adopted at 0 eV. From the BS plot (left Fig. 4 (a)) appraisal of the electronic properties of $B_3O_3$ in various K-mesh points viz. Γ, M, K, can be understood. The lowest unoccupied conduction band (LUCB) and the highest occupied valence band (HOVB) are moved to K (3.634 eV), and Γ (0.0 eV) points, respectively, and this semiconductor nanosheet has $E_g$ of 3.634 eV (Γ-K). Given that PBE functional underrates the $E_g$ amount of 2D-semiconductor, we applied the screened HSE06 hybrid functional [53] to provide more stringent estimations of electronic attributes.

**Table 1.** Adsorption energies in the gas phase ($E_{Ads}^{Gas}$) of dye molecules on a $B_3O_3$ nanosheet, solvation energy ($E_{solv}$), adsorption energy in a water medium ($E_{Ads}^{Solv}$), interaction energies ($E_{int}$), deformation energy of surface ($E_{def/surf}$), deformation energy of dye molecule ($E_{def/dye}$), bandgap ($E_g$), percentage of change in $E_g$ ($\%\Delta E_g$).

| System | | | $E_{Ads}^{Gas}$ (eV) | $E_{solv}$ (eV) | $E_{Ads}^{Solv}$ (eV) | $E_{int}$ (eV) | $E_{def/surf}$ (eV) | $E_{def/dye}$ (eV) | $E_g$ (eV) | $\%\Delta E_g$ |
|---|---|---|---|---|---|---|---|---|---|---|
| Dye | trans | | - | -0.58 | - | - | - | - | 1.809 | - |
| | cis | | - | -0.68 | - | - | - | - | 1.704 | - |
| $B_3O_3$ nanosheet | | | - | -1.43 | - | - | - | - | 3.634 | - |
| Dye/$B_3O_3$ complexes | trans | S1 | -1.48 | -1.56 | -1.03 | -1.65 | 0.09 | 0.08 | 1.803 | 50.4 |
| | | S2 | -0.62 | -1.77 | -0.39 | -1.69 | 0.83 | 0.24 | 1.610 | 55.7 |
| | | S3 | -0.53 | -1.78 | -0.30 | -0.70 | 0.08 | 0.09 | 1.763 | 51.5 |
| | | S4 | -0.25 | -1.80 | -0.05 | -0.38 | 0.05 | 0.07 | 1.804 | 50.4 |
| | cis | S´1 | -1.41 | -1.56 | -0.85 | -1.55 | 0.06 | 0.08 | 1.771 | 51.3 |
| | | S´2 | -0.98 | -2.16 | -1.03 | -1.86 | 0.79 | 0.08 | 1.549 | 57.4 |
| | | S´3 | -0.62 | -2.22 | -0.73 | -0.79 | 0.11 | 0.06 | 1.551 | 57.3 |

We used the CASTEP code [54] in the Materials Studio package. Recently, numerous research has been approved to be more proper HSE06 functional to more accurately assess the electronic attributes of the semiconductors [43, 58, 59]. The $E_g$ of 5.04 eV for the $B_3O_3$ via the HSE06 function aligns with a previous study [27]. After the adsorption of the dye molecule on $B_3O_3$, the $E_g$ values of complex systems considerably decrease as compared to the bare substrate from 3.634 (nanosheet) to 1.803 (50.4%), 1.610 (55.7%), 1.763 (51.5%), 1.804 (50.4%), 1.771 (51.3%), 1.549 (57.4%), and 1.551 (57.3%) for S1, S2, S3, S4, S´1, S´2, S´3 complexes, respectively. The $\%\Delta E_g$ in the cis-dye forms is higher than in trans-dye forms. It is clear from Figure 4; the BS plots include the $B_3O_3$ semiconductor and the dye molecule.

Some of the states of this band structure come from the semiconductor, and the others are from the dye molecule. If we compare this figure with the band structure of the $B_3O_3$ in Fig. 4 (a), we can say that vast peaks are coming from the semiconductor $B_3O_3$. Some are within the semiconductor bands, but the state within the band gap of the complex system's band structure comes from the dye molecule, suitable as a photoanode for the DSSCs application. Maximum $\%\Delta E_g$ is for the S´2 (cis-dye form) complex (57.4%), with the highest interaction among all possible configurations. Therefore, adsorbing the dye on the surface creates bands in the conduction band that reduce the gap energy of the complex, and less energy is needed to excite the electron from the OVB to the UCB band. The adsorption of the dye molecule causes significant changes in the electronic properties of the desired nanosheet.

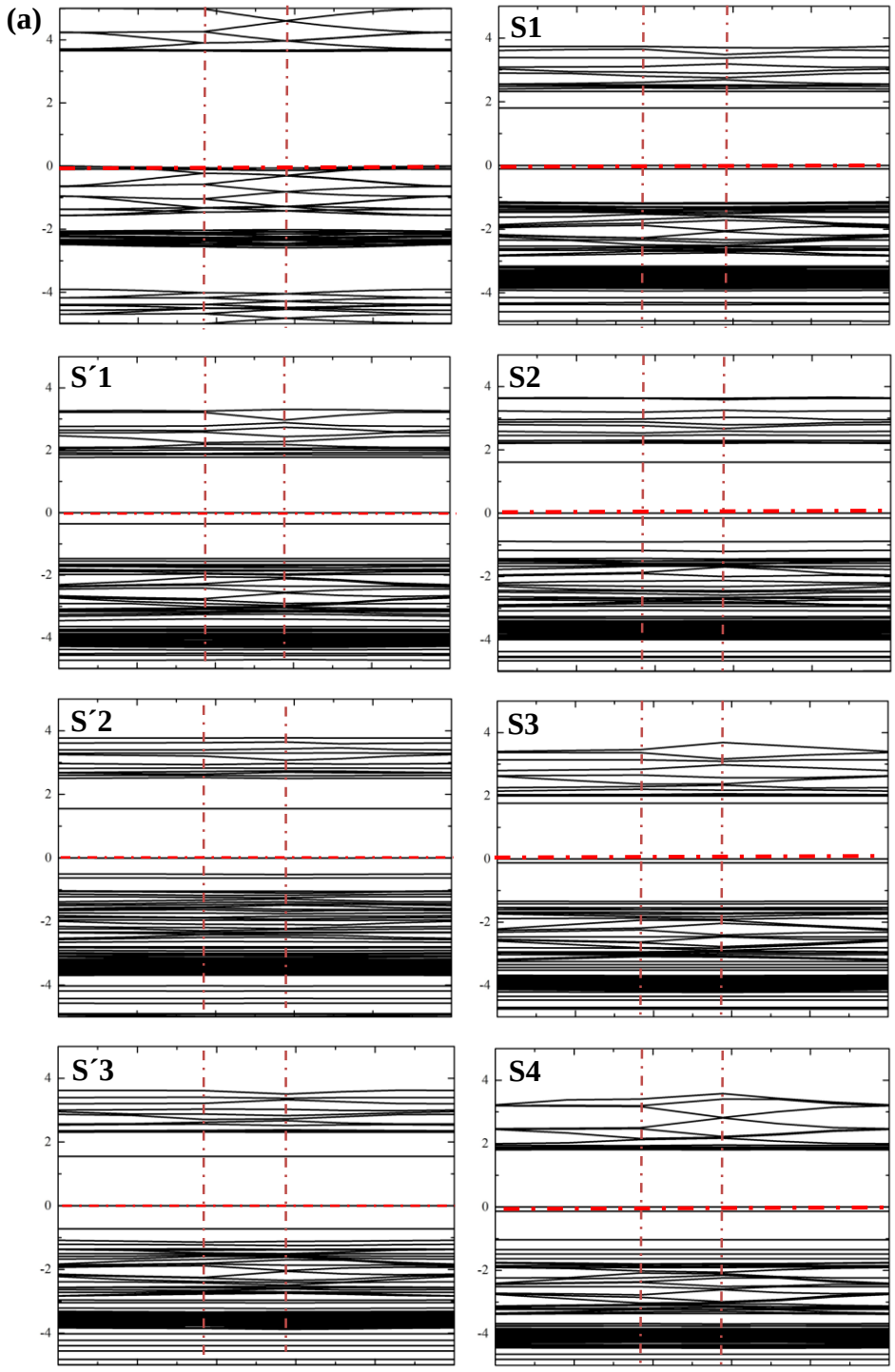


**Figure 4** Band structures (BS) of (a) pristine $B_3O_3$ nanosheet and four and three stable configurations of dye molecule of (S1-S4) trans-P-methyl red and (S´1- S´3) cis-P-methyl red adsorbed on the $B_3O_3$ nanosheet. The red horizontal dash-dotted line displays the position of the Fermi level at 0 eV.

Since the dye remains at S1 and S'1 configuration in the most stable possible states, we examine the effectiveness of dye uptake on the electronic properties of the $B_3O_3$ nanosheet with PDOS analyses on the S1 and S'1 complexes (see Figure 5). The partial density of state (PDOS) plots for (a) S1 complex, (a') S'1 complex, (b) $B_3O_3$ nanosheet in the absence of dye, (c) trans-P-methyl red, and (c') cis-P-methyl red dye molecule in the absence of nanosheet plotted in the energy range of -9 eV to 3 eV. The intensity of *s*, *p*, and *d* orbitals peaks is $p > s > d$. The trans/cis form of the dye molecule has a recognizable peak related to the *p* orbital in the area of -0.05/-0.05 eV (OVB) and 1.84/1.71 eV (UCB) and a feeble peak related to *the s* orbital in the zone of -5.41/-5.67 eV in the (c/c') PDOS plots in Figure 5. Such peaks are not seen in the PDOS plot of the nanosheet (see Fig. 5 (b)). Excitation of the electron occurs from the *p* orbital (OVB) to the *p* orbital of the UCB in the S1 and S'1 configuration (see Figure 5 (a and a')). The complexes' peaks in the UCB zone are due to dye adsorption. The density of state in the LUCB and HOVB levels are changed substantially close to the Fermi level after the interaction of the dye molecule on the $B_3O_3$ nanosheet (see Fig. 5 (a, a', and b)). From the results of analyzes of BS and PDOS, it can be fully understood that the dye adsorption on the surface has led to peaks in the UCB area, which reduces the band gap in the complex, and the electron is more easily excited from the OVB to the UCB. Therefore, the studied nanosheet has an electronic response and a unique sensitivity to p-methyl red dye absorption.

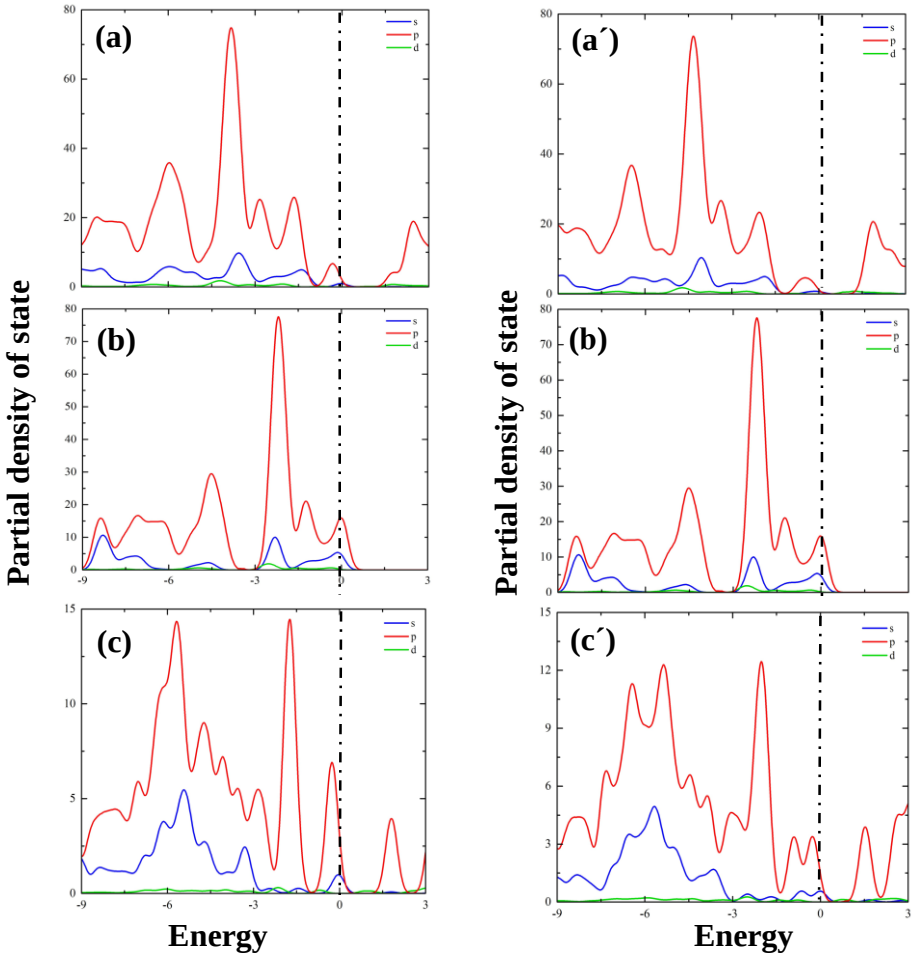


**Fig. 5.** The partial density of state (PDOS) plots for (a) S1 complex, (a´) S´1 complex, (b) $B_3O_3$ nanosheet in the absence of dye, (c) trans-P-methyl red, and (c´) cis-P-methyl red dye molecule in the absence of nanosheet. The blue, red, and green plots represent the *s*, *p*, and *d* orbitals.

## 3. 3. Dye molecules adsorption on the $B_3O_3$ surface in an aqueous medium

To appraise the solubility of the studied systems in an aqueous medium, computations were carried out in water media by COSMO approach [56, 57] that was implemented in DMol$^3$. Thus, we have also investigated the solubility of the dye molecule, $B_3O_3$, and dye/$B_3O_3$ complexes by solvation energy ($E^{Solv}$), which means the difference between the system's total energy in the solvent and gas phases. The $E_{Ads}^{Solv}$ is adsorption energy in an aqueous medium, and the $E_{complex\text{-}hyd}$, $E_{sheet\text{-}hyd}$, and $E_{dye\text{-}hyd}$ are system energy in the water phase for complex, sheet, and dye, respectively. After that, the $E_{Ads}^{Solv}$ can be calculated separately from the following two equations, which are equivalent [60]:

$$E_{Ads}^{Solv} = E_{complex\text{-}hyd} - E_{sheet\text{-}hyd} - E_{dye\text{-}hyd} \quad (4)$$

$$E_{Ads}^{Solv} = E_{Ads}^{Gas} + E_{complex}^{Solv} - E_{sheet}^{Solv} - E_{dye}^{Solv} \quad (5)$$

The $E_{Ads}^{Solv}$ of S1, S2, S3, S4, S´1, S´2, and S´3 complexes calculated -1.03, -0.39, -0.30, -0.05, -0.85, -1.03, and -0.73 eV, respectively (see Table 1). The $B_3O_3$, trans-dye, cis-dye, S1, S2, S3, S4, S´1, S´2, S´3 complexes ' solvation energies have been computed at -1.43, -0.58, -0.68, -1.56, -1.77, -1.78, -1.80, -1.56, -2.16 and -2.22 eV, respectively. Overall, the $E_{Ads}^{Solv}$ , $E^{Solv}$, and $\%\Delta E_g$ for cis-isomer is greater than trans-isomer. In contrast, the stability of the trans-isomer is greater than the cis-isomer.

It is time to compare the present work results with similar reported results. The energy of the BrPDI, BrGly, and BrAsp dyes adsorption on the $TiO_2$ surface is about 2.3-3.1 eV [17]. The highest adsorption energy of the cyanidin glucoside and TA-St-CA dye molecules on (001) / (101) $TiO_2$ surfaces are -1.67/-2.59, and -1.05/-0.84 eV, respectively [18]. The coumarin, tetrahydroquinoline with two monodentate and bidentate bonding modes of dye molecules are adsorbed on the anatase (001)/(101) $TiO_2$ surfaces with an adsorption energy of -0.46 /-0.63, -0.72, and -1.36 /-0.57 and -0.94 eV, respectively [19]. In the present study, the maximum $E_{Ads}^{Gas}$ of the dye/$B_3O_3$ complexes is -1.48 eV (trans-isomer) and –1.41 eV (cis-isomer) with $\%\Delta E_g$ in the range of 50 to 57% and excellent electronic response to p-methyl red dye molecule adsorption. The strength of our work is that we have introduced a pristine synthesized nanostructure without any structural manipulation as a potential semiconductor photoanode. In comparison, adsorption of the same dye molecule on the (101) $TiO_2$ surface is obtained a-0.6 eV [20] and -0.16 eV [21], respectively. Although the maximum $\%\Delta E_g$ for (101) $TiO_2$ gains 72%, the desired dye molecule is weaker and adsorbed on (101) $TiO_2$ than our studied $B_3O_3$ nanosheet. The advantage of our work over these two similar works is that we have thoroughly studied the adsorption of P-methyl red dye molecule in both trans and cis configurations. In contrast, they have only analyzed the trans configuration of the p-methyl red dye molecule. So, a few configurations have been ignored. This indicates that our desired pristine $B_3O_3$ nanosheet is a wonderful substrate for the adsorption of p-methyl red dye molecules.

## 4. Conclusions

First-principal calculations were utilized to study complexes of the pristine $B_3O_3$ nanosheet with 4- [2- [4-(dimethyl amino) phenyl] diazinyl]-benzoic acid dye molecule in two trans and cis forms. The considered dye molecule is adsorbed on the $B_3O_3$ surface via the association between the carboxylic acid group and N atoms of the dye molecule with appropriate B and O atoms of the surface with maximum adsorption energy -1.48 eV (trans form) and –1.41 eV (cis form). The band gap of the $B_3O_3$ sheet has been changed dramatically with a maximum of 55% (trans form) and 57% (cis form) due to the interaction with the picked dye molecule in this investigation. Overall, the stability of the trans-dye molecule form is more significant than the cis-dye molecule form. In contrast, the $E_{int}$, $E_{Ads}^{Solv}$ , $E^{Solv}$, and $\%\Delta E_g$ for cis-dye configuration is more significant than trans-dye configuration. We hope that the present research results can be effective in practice in fabricating high-performance adsorbent based on synthesized pristine $B_3O_3$ nanosheet as an alternative in dye-sensitized solar cells.

## Conflicts of Interest

The author declares no conflict of interest.

## Author information

*Corresponding Author: Rezvan Rahimi, Mohammad Solimannejad

E-mail addresses: r.rahimi1989@gmail.com and m-solimannejad@araku.ac.ir

## ORCID

Mohammad Solimannejad: 0000-0003-0617-8689

## References

[1] J.M. Pearce, Photovoltaics—a path to sustainable futures, Futures 34 (2002) 663-674. https://doi.org/10.1016/S00163287(02)000083.
[2] B. O'regan, M. Grätzel, A low-cost, high-efficiency solar cell based on dye-sensitized colloidal $TiO_2$ films, nat. 353 (1991) 737-740. https://doi.org/10.1038/353737a0.
[3] M. Grätzel, Dye-sensitized solar cells, J. Photochem. Photobiol., C. 4 (2003) 145-153. https://doi.org/10.1016/S1389-5567(03)00026-1.
[4] M. Grätzel, Recent advances in sensitized mesoscopic solar cells, Acc. Chem. Res. 42 (2009). 1788-1798. https://doi.org/10.1021/ar900141y.
[5] M.K. Nazeeruddin, F. De Angelis, S. Fantacci, A. Selloni, G. Viscardi, P. Liska, S. Ito, B. Takeru, M. Grätzel, Combined experimental and DFT-TDDFT computational study of photoelectrochemical cell ruthenium sensitizers, J. Am. Chem. Soc. 127 (2005) 16835-16847. https://doi.org/10.1021/ja052467l.
[6] S. Kim, J.K. Lee, S.O. Kang, J. Ko, J.-H. Yum, S. Fantacci, F. De Angelis, D. Di Censo, M.K. Nazeeruddin, M. Grätzel, Molecular engineering of organic sensitizers for solar cell applications, J. Am. Chem. Soc. 128 (2006) 16701-16707. https://doi.org/10.1021/ja066376f.
[7] A. Hagfeldt, G. Boschloo, L. Sun, L. Kloo, H. Pettersson, Dye-sensitized solar cells, Chem. Rev. 110 (2010) 6595-6663. https://doi.org/10.1021/cr900356p.
[8] A.B. Muñoz-García, I. Benesperi, G. Boschloo, J.J. Concepcion, J.H. Delcamp, E.A. Gibson, G.J. Meyer, M. Pavone, H. Pettersson, A. Hagfeldt, Dye-sensitized solar cells strike back, Chem. Soc. Rev. 50 (2021) 12450-12550. https://doi.org/10.1039/D0CS01336F.
[9] F. Freitas, A. Gonçalves, A. Morais, J. Benedetti, A. Nogueira, Graphene-like $MoS_2$ as a low-cost counter electrode material for dye-sensitized solar cells, Nano. J. Ener. Sust. 1 (2013) 011002.
[10] C. Cavallo, F. Di Pascasio, A. Latini, M. Bonomo, D. Dini, Nanostructured semiconductor materials for dye-sensitized solar cells, J. Nanomater. 2017 (2017) 31. https://doi.org/10.1155/2017/5323164.
[11] I. Benesperi, H. Michaels, M. Freitag, The researcher's guide to solid-state dye-sensitized solar cells, J. Mater. Chem. C. 6 (2018) 11903-11942. https://doi.org/10.1039/C8TC03542C.
[12] M. Hajimohammadi, A. Vaziri Sereshk, C. Schwarzinger, G. Knör, Suppressing Effect of 2-Nitrobenzaldehyde on Singlet Oxygen Generation, Fatty Acid Photooxidation, and Dye-Sensitizer Degradation, Antioxidants, 7 (2018) 194. https://doi.org/10.3390/antiox7120194.
[13] W. Maiaugree, S. Lowpa, M. Towannang, P. Rutphonsan, A. Tangtrakarn, S. Pimanpang, P. Maiaugree, N. Ratchapolthavisin, W. Sang-Aroon, W. Jarernboon, A dye sensitized solar cell using natural counter electrode and natural dye derived from mangosteen peel waste, Sci. Rep. 5 (2015) 1-12. https://doi.org/10.1038/srep15230
[14] J.H. Yum, P. Chen, M. Grätzel, M.K. Nazeeruddin, Recent developments in solid-state dye-sensitized solar cells, Chem. Sus. Chem. 1 (2008) 699-707.
https://doi.org/10.1002/cssc.200800084.
[15] M. Law, L.E. Greene, J.C. Johnson, R. Saykally, P. Yang, Nanowire dye-sensitized solar cells, Nat. mater. 4 (2005) 455-459. https://doi.org/10.1038/nmat1387.
[16] B.E. Hardin, H.J. Snaith, M.D. McGehee, The renaissance of dye-sensitized solar cells, Nat. Photonics, 6 (2012) 162-169. https://doi.org/10.1038/nphoton.2012.22.
[17] D. Çakır, O. Gülseren, E. Mete, Ş. Ellialtıoğlu, Dye adsorbates BrPDI, BrGly, and BrAsp on anatase $TiO_2$ (001) for dye-sensitized solar cell applications, Phys. Rev. B. 80 (2009) 035431.
https://doi.org/10.1103/PhysRevB.80.035431.
[18] H. Ünal, D. Gunceler, O. Gülseren, Ş. Ellialtıoğlu, E. Mete, Anatase $TiO_2$ nanowires functionalized by organic sensitizers for solar cells: A screened Coulomb hybrid density functional study, J. Appl. Phys. 118 (2015) 194301. https://doi.org/10.1063/1.4935523.
[19] H. Unal, D. Gunceler, O. Gulseren, S.i. Ellialtıoğlu, E. Mete, Range-separated hybrid density functional study of organic dye sensitizers on anatase $TiO_2$ nanowires, J. Phys. Chem. C. 118 (2014) 24776-24783. https://doi.org/10.1021/jp507899c.

[20] L. Zhang, X. Liu, W. Rao, J. Li, Multilayer Dye Aggregation at Dye/$TiO_2$ Interface via π… π Stacking and Hydrogen Bond and Its Impact on Solar Cell Performance: A DFT Analysis, Sci. Rep. 6 (2016) 1-8. https://doi.org/10.1038/srep35893.
[21] L. Zhang, J.M. Cole, Adsorption properties of p-methyl red monomeric-to-pentameric dye aggregates on anatase (101) titania surfaces: First-principles calculations of dye/$TiO_2$ photoanode interfaces for dye-sensitized solar cells, ACS Appl. Mater. Interfaces. 6 (2014) 15760-15766. https://doi.org/10.1021/am502687k.
[22] R. Rahimi, M. Solimannejad, $B_3O_3$ monolayer: an emerging 2D material for $CO_2$ capture, New J. Chem. 45 (2021) 15328-15335. https://doi.org/10.1039/D1NJ02870G.
[23] R. Rahimi, M. Solimannejad, Z. Ehsanfar, First-principles studies on two-dimensional B3O3 adsorbent as a potential drug delivery platform for TEPA anticancer drug, J. Mol. Model. 27 (2021) 1-10. https://doi.org/10.1007/s00894-021-04930-x.
[24] R. Rahimi, M. Solimannejad, $B_3O_3$ monolayer with dual application in sensing of COVID-19 biomarkers and drug delivery for treatment purposes: A periodic DFT study, J. Mol. Liq. 354 (2022) 118855. https://doi.org/10.1016/j.molliq.2022.118855.
[25] M. Stredansky, A. Sala, T. Fontanot, R. Costantini, C. Africh, G. Comelli, L. Floreano, A. Morgante, A. Cossaro, On-surface synthesis of a 2D boroxine framework: a route to a novel 2D material?, Chem. Commun. 54 (2018) 3971-3973. https://doi.org/10.1039/C8CC01372A.
[26] S. Lin, J. Gu, H. Zhang, Y. Wang, Z. Chen, Porous hexagonal boron oxide monolayer with robust wide band gap: A computational study, Flat. Chem. 9 (2018) 27-32. https://doi.org/10.1016/j.flatc.2018.05.002.
[27] S. Ullah, P.A. Denis, F. Sato, Theoretical investigation of various aspects of two-dimensional holey boroxine, $B_3O_3$, RSC Adv. 9 (2019) 37526-37536. https://doi.org/10.1039/C9RA07338H.
[28] K.M. Lee, D.H. Wang, H. Koerner, R.A. Vaia, L.S. Tan, T.J. White, Enhancement of photogenerated mechanical force in azobenzene-functionalized polyimides, Angew. Chem., Int. Ed. 51 (2012) 4117-4121. https://doi.org/10.1002/anie.201200726.
[29] H.Y. Lee, X. Song, H. Park, M.-H. Baik, D. Lee, Torsionally Responsive C 3-Symmetric Azo Dyes: Azo−Hydrazone Tautomerism, Conformational Switching, and Application for Chemical Sensing, J. Ame. Chem. Soc. 132 (2010) 12133-12144. https://doi.org/10.1021/ja105121z.
[30] W. Feng, W. Luo, Y. Feng, Photo-responsive carbon nanomaterials functionalized by azobenzene moieties: structures, properties and application, Nanoscale. 4 (2012) 6118-6134. https://doi.org/10.1039/C2NR31505J.
[31] J. Mikroyannidis, D. Tsagkournos, P. Balraju, G. Sharma, Low band gap dyes based on 2-styryl-5-phenylazo-pyrrole: Synthesis and application for efficient dye-sensitized solar cells, J. Power Sources. 196 (2011) 4152-4161. https://doi.org/10.1016/j.jpowsour.2010.12.038.
[32] L. Zhang, J.M. Cole, P.G. Waddell, K.S. Low, X. Liu, Relating electron donor and carboxylic acid anchoring substitution effects in azo dyes to dye-sensitized solar cell performance, ACS Sustainable Chem. Eng. 1 (2013) 1440-1452. https://doi.org/10.1021/sc400183t.
[33] B. Delley, An all-electron numerical method for solving the local density functional for polyatomic molecules, J.chem. phys. 92 (1990) 508-517. https://doi.org/10.1063/1.458452.
[34] B. Delley, Fast calculation of electrostatics in crystals and large molecules, J. phys. chem. 100 (1996) 6107-6110. https://doi.org/10.1021/jp952713n.
[35] B. Delley, From molecules to solids with the DMol 3 approach, J.chem. phys. 113 (2000) 7756-7764. https://doi.org/10.1063/1.1316015.
[36] J.P. Perdew, J.A. Chevary, S.H. Vosko, K.A. Jackson, M.R. Pederson, D.J. Singh, C. Fiolhais, Atoms, molecules, solids, and surfaces: Applications of the generalized gradient approximation for exchange and correlation, Phys. rev. B. 46 (1992) 6671. https://doi.org/10.1103/PhysRevB.46.6671.
[37] H. Zhang, W.-X. Li, First-principles investigation of surface and subsurface H adsorption on Ir (111), J. Phys. Chem. C. 113 (2009) 21361-21367. https://doi.org/10.1021/jp9074866.
[38] S. Grimme, Semiempirical GGA-type density functional constructed with a long-range dispersion correction, J. comput. chem. 27 (2006) 1787-1799. https://doi.org/10.1002/jcc.20495.
[39] E. Kim, P.F. Weck, S. Berber, D. Tománek, Mechanism of fullerene hydrogenation by polyamines: Ab initio density functional calculations, Phys. Rev. B. 78 (2008) 113404. https://doi.org/10.1103/PhysRevB.78.113404.
[40] R. Rahimi, M. Solimannejad, High-Performance Hydrogen Storage Properties of Li-Decorated B2N2 Nanosheets: A Periodic Density Functional Theory Study, Energy Fuels, 35 (2021) 6858–6867. https://doi.org/10.1021/acs.energyfuels.1c00246.

[41] R. Rahimi, M. Solimannejad, Periodic DFT insights into hydrogen storage of a $B_4CN_3$ nanosheet, New J. Chem. 45 (2021) 2463-2469. https://doi.org/10.1039/D0NJ05652A.
[42] R. Rahimi, M. Solimannejad, A. Chaudhari, Pristine $B_3CN_4$ monolayer for hydrogen storage: A first-principles approach, Phys. Lett. A. 391 (2021) 127116. https://doi.org/10.1016/j.physleta.2020.127116.
[43] R. Rahimi, M. Solimannejad, A. Chaudhari, Toxic volatile organic compounds sensing by Al2C monolayer: A first-principles outlook, J. Hazard. Mater. 403 (2021) 123600. https://doi.org/10.1016/j.jhazmat.2020.123600.
[44] R. Rahimi, M. Solimannejad, Hydrogen storage on pristine and Li-decorated BC6N monolayer from first-principles insights, Mol. Phys. 119 (2021) e1827177. https://doi.org/10.1080/00268976.2020.1827177.
[45] R. Rahimi, M. Solimannejad, Li-decorated $Al_2C$ monolayer as a potential template for hydrogen storage: A first-principles perspective, Int. J. Quantum Chem. 121 (2021) e26528. https://doi.org/10.1002/qua.26528.
[46] R. Rahimi, M. Solimannejad, First-principles survey on the pristine BC2N monolayer as a promising vehicle for delivery of β-lapachone anticancer drug, J. Mol. Liq. 321 (2021) 114917. https://doi.org/10.1016/j.molliq.2020.114917.
[47] R. Rahimi, M. Solimannejad, First-principles study of superior hydrogen storage performance of Li-decorated Be2N6 monolayer, Int. J. Hydrogen Energy. 45 (2020) 19465-19478. https://doi.org/10.1016/j.ijhydene.2020.05.047.
[48] R. Rahimi, M. Solimannejad, M. Farghadani, Adsorption of chloroquine and hydroxychloroquine as potential drugs for SARS-CoV-2 infection on BC 3 nanosheets: a DFT study, New J. Chem. 45 (2021) 17976-17983. https://doi.org/10.1039/D1NJ03084A.
[49] R. Rahimi, M. Solimannejad, BC3 graphene-like monolayer as a drug delivery system for nitrosourea anticancer drug: A first-principles perception, Appl. Surf. Sci. 525 (2020) 146577. https://doi.org/10.1016/j.apsusc.2020.146577.
[50] R. Rahimi, M. Solimannejad, Gas-sensing performance of BC 3 nanotubes for detecting poisonous cyanogen gas: a periodic DFT approach, New J. Chem. 45 (2021) 11574-11584. https://doi.org/10.1039/D1NJ01977E.
[51] R. Rahimi, M. Solimannejad, Sensing ability of 2D Al2C monolayer toward toxic pnictogen hydrides: A first-principles perspective, Sens. Actuators, A. 331 (2021) 113000. https://doi.org/10.1016/j.sna.2021.113000.
[52] R. Rahimi, M. Solimannejad, Z. Ehsanfar, High sensitivity of 2D covalent triazine framework for recognition of NO, NO2, and HO2 radicals: A periodic DFT study, Chem. Phys. Lett. 805 (2022) 139940. https://doi.org/10.1016/j.cplett.2022.139940.
[53] R. Rahimi, M. Solimannejad, M. Soleimannejad, Two-dimensionalcovalent triazine frameworks as superior nanocarriers for the delivery of thioguanine anti-cancer drugs: a periodic DFT study, New J. Chem. 46 (2022) 15635-15644. https://doi.org/10.1039/D2NJ02050E.
[54] R. Rahimi, M. Solimannejad, Empowering hydrogen storage performance of B4C3 monolayer through decoration with lithium: A DFT study, Surf. Interfaces. 29 (2022) 101723. https://doi.org/10.1016/j.surfin.2022.101723.
[55] R. Rahimi, M. Solimannejad, Z. Ehsanfar, Potential application of XC3 (X= B, N) nanosheets in drug delivery of hydroxyurea anticancer drug: a comparative DFT study, Mol. Phys. 120 (2022) e2014587. https://doi.org/10.1080/00268976.2021.2014587.
[56] A. Klamt, G. Schüürmann, COSMO: a new approach to dielectric screening in solvents with explicit expressions for the screening energy and its gradient, J. Chem. Soc. 2 (1993) 799-805. https://doi.org/10.1039/P29930000799.
[57] A. Klamt, Conductor-like screening model for real solvents: a new approach to the quantitative calculation of solvation phenomena, J. Phys. Chem. 99 (1995) 2224-2235. https://doi.org/10.1021/j100007a062.
[58] M. Ghambarian, Z. Azizi, M. Ghashghaee, Remarkable improvement in phosgene detection with a defect-engineered phosphorene sensor: first-principles calculations, Phys. Chem. Chem. Phys. 22 (2020) 9677-9684. https://doi.org/10.1039/D0CP00427H.
[59] M. Ghashghaee, M. Ghambarian, Highly improved carbon dioxide sensitivity and selectivity of black phosphorene sensor by vacancy doping: A quantum chemical perspective, Int. J. Quantum Chem. 120 (2020) e26265. https://doi.org/10.1002/qua.26265.
[60] M.-H. Ri, Y.-M. Jang, U.-S. Ri, C.-J. Yu, K.-I. Kim, S.-U. Kim, Ab initio investigation of adsorption characteristics of bisphosphonates on hydroxyapatite (001) surface, J. Mater. Sci. 53 (2018) 4252-4261. https://doi.org/10.1007/s10853-017-1880-1.